



# Effect of working fluids on the performance of phase change material storage based direct vapor generation solar organic Rankine cycle system



Jahan Zeb Alvi <sup>a</sup>, Yongqiang Feng <sup>a,\*</sup>, Qian Wang <sup>a,\*</sup>, Muhammad Imran <sup>b</sup>, Gang Pei <sup>c</sup>

<sup>a</sup> School of Energy and Power Engineering, Jiangsu University, 301 Xuefu Road, Zhenjiang, China

<sup>b</sup> School of Engineering and Applied Science, Aston University, Aston Triangle, B4 7ET, Birmingham, UK

<sup>c</sup> Department of Thermal Science and Energy Engineering, University of Science and Technology of China, China

## ARTICLE INFO

### Article history:

Received 10 July 2020

Received in revised form 27 November 2020

Accepted 28 December 2020

Available online xxxx

### Keywords:

Solar organic Rankine cycle

Direct vapor generation

Phase change material

Efficiency

Working fluids

Energy stored

## ABSTRACT

Working fluids can play a critical role in the working of an organic Rankine cycle system. A direct vapor generation solar organic Rankine cycle embedded with phase change material storage is analyzed in this study. The system comprised of an array of evacuated flat plate collectors, phase change material based thermal storage, expander, condenser, and organic working fluid pump. The storage tank model is modeled using a finite difference method in MATLAB programming environment while the 1D model of ORC system is used to evaluate the system performance. After a careful screen, 12 dry and isentropic working fluids were selected and their impact on the performance of the heat storage tank and the overall system is evaluated. The results show that the system efficiencies increase and decrease with the increment and decrement in the critical temperature of the working fluid. Moreover, the rise and fall of working fluid temperature, phase change material temperature, and the quantity of energy stored and released generally increase with an increase in the critical temperature of the working fluid. At the evaporation temperature of 10 °C higher and lower than the melting point temperature of the phase change material, Benzene has achieved the highest system efficiencies of 10.7% & 10.4% during charging and discharging mode, respectively. However, the maximum the rise and fall of working fluid temperature, phase change material temperature, and the quantity of energy stored and released during charging and discharging mode is attained by Heptane which is found to be 5.35 °C & 7.34 °C, 0.48 °C & 0.44 °C and 13.81 MJ & 23.04 MJ, respectively. Heptane has shown overall best performance among the selected working fluids and found to be feasible for phase change material storage based direct vapor generation solar ORC system.

© 2020 The Author(s). Published by Elsevier Ltd. This is an open access article under the CC BY-NC-ND license (<http://creativecommons.org/licenses/by-nc-nd/4.0/>).

## 1. Introduction

Energy demand per capita is increasing day by day due to an increase in the human population at a high rate. Therefore, along with high-grade heat, low-grade heat conversion has received significant attention in the recent past. Solar thermal energy is one of the potential sources of low-grade heat. There have been different technologies reported in the past to convert low-grade heat into power such as Kalina cycle (Ghaebi and Rostamzadeh, 2020), Goswami cycle (Sayyaadi et al., 2020), trilateral flash cycle (Iqbal et al., 2020), Stirling cycle and the organic Rankine cycle (Li et al., 2016b). The organic Rankine cycle (ORC) seems to be one of the most favorable and promising technology for low to medium heat applications.

The organic Rankine cycle works on the same principle as the steam Rankine cycle. An organic fluid has low boiling point temperature, and high molecular mass is used as working fluid instead of water in an ORC system. The ORC is advantageous because of its smaller unit size, higher thermal efficiency during cold ambient temperature, application for the remote area and suitability for cogeneration (Usman et al., 2017). The organic Rankine cycle powered by solar thermal energy can be an attractive option to convert solar radiation into power (Oyekale et al., 2020; Refiei et al., 2020). However, the intermittent nature of solar radiation can cause a hindrance to this process. Therefore, thermal storage is generally employed in the system to bring stability in power generation (Alvi et al., 2017).

Solar organic Rankine cycle system is generally divided into two kinds of systems, namely direct vapor generation (DVG) solar ORC system and indirect or conventional solar ORC system. The DVG solar ORC system is the one in which an intermediate heat exchanger is removed, and the solar thermal collectors act as an

\* Corresponding authors.

E-mail addresses: [hitfengyq@gmail.com](mailto:hitfengyq@gmail.com) (Y. Feng), [qwang@ujs.edu.cn](mailto:qwang@ujs.edu.cn) (Q. Wang).

evaporator. However, in the case of an indirect or conventional solar ORC system, heat transfer fluid (HTF) is used to carry heat from solar collectors to the working fluid through the intermediate heat exchanger. The DVG solar ORC system is advantageous in comparison with the indirect solar ORC system due to its higher thermal efficiency, less complexity and low cost (Xu et al., 2015).

The DVG solar ORC system has achieved significant attention in the recent past. The previous studies on the system include both theoretical studies (Li et al., 2016a; Bu et al., 2013; Wang et al., 2010) as well as experimental work (Wang et al., 2011, 2012). It has been found that HTF based or indirect solar ORC system is less efficient, more complex and more costly than the DVG system. Conversely, regulation and control of the indirect system are much easier as compared to the DVG system (Quoilin et al., 2011). However, the evaporation process inside the collector tube becomes more complicated for the DVG system. Moreover, DVG solar ORC system is highly sensitive to environmental conditions such as ambient temperature and solar radiation (Marion et al., 2014). Therefore, solar collector selection and the impact of working fluids become more critical for the DVG system.

The solar collectors are an integral part of a DVG solar ORC system. There are two types of collectors employed in the system, namely concentrating and non-concentrating solar collectors. The concentrating collectors utilize beam solar radiations, while non-concentrating collectors use both diffused and beam solar radiations (Gang et al., 2011). The solar collectors in DVG solar ORC system work at high pressure and temperature. Therefore, the collectors designed to work at high pressure and temperature are considered to be feasible for DVG application. Solar collectors like compound parabolic concentrators, parabolic trough collectors and evacuated tube heat pipe collectors can be suitable candidates for DVG solar ORC system (Li et al., 2015; Tian and Zhao, 2013). However, an evacuated flat plate collector (EFPC) has been reportedly utilized for DVG application because of its high efficiency at high operating temperature and pressure. An EFPC collector can achieve a thermal efficiency of 50% while operating at 200 °C temperature. This kind of collector is also advantageous because of its non-concentrating and non-tracking nature (Calise et al., 2015).

To stabilize the operation of the DVG solar ORC system, thermal storage is generally employed. Thermal storages are divided into sensible thermal storages (STS) and latent heat thermal storages (LTS) (Tian and Zhao, 2013). A phase change material (PCM) storage is a type of LTS and generally preferred for DVG solar ORC system. This kind of storage is advantageous because of its maximum energy storage at nearly isothermal temperature and high energy density. The phase change materials (PCMs) can absorb 5 to 14 times extra heat per unit volume in comparison with sensible heat storages (Sharma et al., 2009). However, there are some drawbacks of PCMs such as flammability, sub-cooling and low thermal conductivity (Hasnain, 1998). The PCMs can also be divided based on their melting point temperature, such as high-temperature PCMs (>150 °C), medium temperature PCMs (60–150 °C), and low-temperature PCMs (<60 °C). The PCMs lies in the range of medium temperature are generally preferred for the solar ORC systems (Agyenim et al., 2010).

Integration of solar ORC system with PCMs have received significant attention in the last decade. Gang et al. (2011) and Pei et al. (2010) analyzed the two-staged PCMs based solar ORC system. The collector and cycle efficiency have been evaluated. The employment of two-staged PCMs had increased heat transfer between PCM and working fluid. Manfrida et al. (2016) and Lakhani et al. (2017) have done simulation and modeling of PCMs for 7 and 10 days, respectively. In the first study, it was found that PCM container having a smaller diameter and longer length result in better system performance. Similarly, in the second study, it was

found that the PCM storage tank has shown 10% higher efficiency during charging mode as compared to discharging mode.

Freeman et al. (2017) and Iasiello et al. (2017) have compared the effect of different PCMs on solar ORC system. The first study concentrated on the comparison of organic PCMs, inorganic PCMs and water storage based solar ORC systems. It was found that PCMs storage based solar ORC system has achieved 20% extra electrical output per unit volume in comparison with the water storage based solar ORC system. In the second study, thermal analysis and comparison of two PCMs, namely Erythritol and  $\text{MgCl}_2 \cdot 6\text{H}_2\text{O}$ , was carried out. The results had shown that Erythritol could store 30% extra energy per unit volume as compared to  $\text{MgCl}_2 \cdot 6\text{H}_2\text{O}$ .

Solar salt was used as PCM storage in a solar ORC system of 100 kW thermal capacity (Costa et al., 2018; Costa et al., 2020). The results had shown that the temperature gradient across the PCM storage tank decrease with the use of aluminum fins. Alvi et al. (2017, 2019) compared and analyzed the PCM based DVG and indirect solar ORC systems. It was found that the thermal match between PCM and the working fluid is much stronger than that between water and PCM. However, energy stored per unit volume in the indirect solar ORC system is more abundant than the DVG solar ORC system.

The previous studies on PCM based solar ORC system were generally focused on simulation, modeling and performance evaluation. Furthermore, most of the studies were based on an indirect solar ORC system, and a limited number of working fluids were investigated. Moreover, the detailed research on the effect of different working fluids on PCM storage incorporated in the DVG solar ORC system has not yet been analyzed. The novelty of the present work lies in the performance evaluation of PCM storage incorporated in the DVG solar ORC system using 12 different working fluids. The contribution includes

- The development and validation of the PCM storage tank model with numerical and experimental data.
- The effect of evaporation temperature of the working fluid, mass flow rate of working fluid and length of PCM tube on the overall system's performance.
- The evaluation and comparison of system efficiency all along with the charging and discharging process of the PCM, respectively.
- The evaluation and comparison of rise and fall in working fluid and PCM temperatures, the quantity of heat stored and released by the PCM during charging and discharging mode.

This study can act as a bench reference for the future work in the area of solar ORC system with integrated phase change material storage. It will facilitate the design engineers to select the suitable working fluid based on its performance for the PCM incorporated DVG solar ORC system.

## 2. System description

A layout diagram of the PCM based DVG solar ORC system is presented in Fig. 1. The system is comprised of an array of high-efficiency EFPC solar thermal collectors, a cylindrical heat storage tank, an expander, a condenser and an organic fluid pump. The array of EFPC solar thermal collectors operates as an evaporator or direct vapor generator in the system. The storage tank operates in two modes, namely charging and discharging mode, respectively. Furthermore, a basic DVG solar ORC system is considered because of its simple control and less complexity.

The system works in two modes of operation:

1. If the melting point temperature of the PCM is kept lower than the evaporation temperature of the working fluid. Then the system lies in charging mode ( $T_{\text{evp}} > T_m$ ).

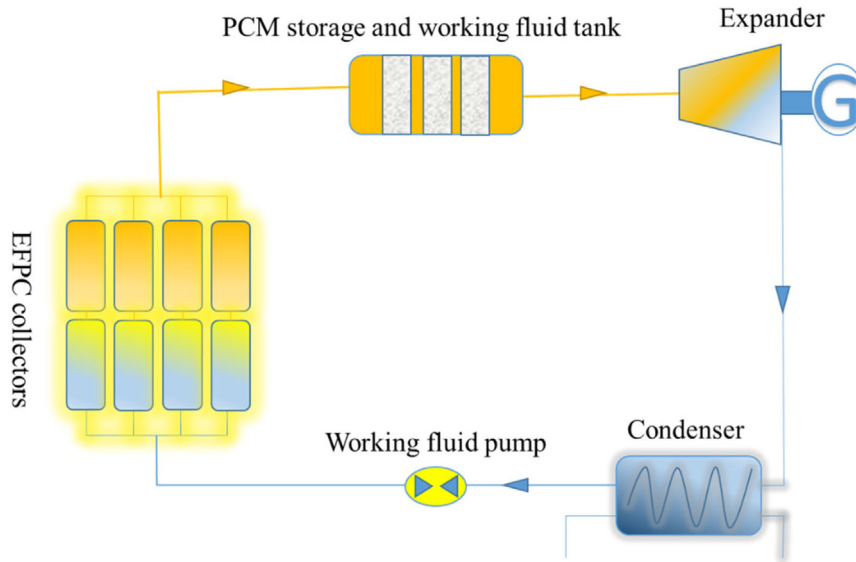


Fig. 1. The layout diagram of the phase change material storage-based DVG solar ORC system.

- If the melting point temperature of the PCM is kept higher than the evaporation temperature of the working fluid. Then the system lies in discharging mode ( $T_{evp} < T_m$ ).

The whole process consists of evaporation, expansion, condensation and pressurization. The working fluid is firstly heated up to specified evaporation temperature in an array of EFPC solar thermal collectors. The collectors collect energy from solar radiation and carry it to the working fluid. Then the working fluid passes through the PCM storage tank to either absorb heat during charging mode or extract heat during discharging mode. The working fluid then enters the expander in a saturated vapor phase to deliver power output while dropping the pressure. Afterward, it is condensed in the condenser to the subcooled liquid phase. Finally, the working fluid pump is employed to pressurize in the working fluid to transfer it back to the solar collectors.

The initial temperature of PCM is assumed to be 10 °C lower than the melting point of the PCM. This shows that PCM is not charged and in the solid phase at the beginning of the simulation process. The discharging limit of the storage tank is maintained to 20 °C lower than the melting point of the PCM, which means that the system is allowed to discharge the storage in a sensible heat region. Moreover, the discharging continue directly after a charging process.

### 3. Thermodynamic modeling

#### 3.1. The solar radiation collection system

To efficiently harness the available solar radiation, an evacuated flat plate collectors (EFPCs) array is employed in the DVG solar ORC system.

This type of collector is beneficial for the area having less solar resource because it utilizes both beam and diffused solar radiations, respectively. Furthermore, it can work efficiently at high operating temperatures and can withstand high operating pressures. Moreover, it is a non-concentrating and non-tracking solar collector with minimal control requirements (Calise et al., 2015). The heat loss formula is commonly used to derive the efficiency of a solar thermal collector.

$$\eta_{cl}(T) = \eta_{cl,0} - \frac{A}{G}(T - T_{amb}) - \frac{B}{G}(T - T_{amb})^2 \quad (1)$$

where the optical efficiency  $\eta_{cl,0}$  is 0.774, primary heat loss coefficient  $A$  of solar collectors is  $0.376 \text{ Wm}^{-2} \text{ }^\circ\text{C}^{-1}$  and the secondary heat loss coefficient  $B$  is  $0.006 \text{ Wm}^{-2} \text{ }^\circ\text{C}^{-2}$  (Freeman et al., 2017; TVP Solar Datasheet, 2020). For instantaneous efficiency a standard value of irradiance shell in tube heat exchanger of  $1000 \text{ W/m}^2$  is chosen in present study. The heat loss equation is suitable for the efficiency calculation of a single unit of solar thermal collector having a surface area of 1–2  $\text{m}^2$ . However, in the case of hundreds and thousands of units, the temperature difference in neighboring collectors is small. Hence, the average temperature of the collector varies from one unit to next. The organic fluid goes into the collector array in the liquid phase while it exists in the binary or vapor phase. Therefore, it is appropriate to compute the collector's efficiency in the binary phase by using a heat loss formula because the temperature remains constant during the binary phase. Conversely, the average temperature of the collector varies significantly during the liquid phase. Hence, the thermal efficiency of the solar collector during the liquid phase is computed as follows:

The surface area of the solar thermal collector in the liquid phase is computed by Eq. (2) (Li et al., 2016a).

$$S_l = \int_{T_{f,i}}^{T_{f,o}} \frac{m_f C_{p,f}(T)}{\eta_{cl}(T)G} dT \quad (2)$$

The specific heat of organic fluid is computed by using a first-order approximation

$$C_p(T) = C_{p,0} + \alpha(T - T_0) \quad (3)$$

By putting  $a_1 = A/G$ ,  $a_2 = B/G$ , the solar collector area can be computed by using Eqs. (1), (2) and (3)

$$S_l = \frac{m_f}{c_2 G (\theta_2 - \theta_1)} \left[ (C_{p,0} + \alpha\theta_1) \ln \frac{(T_{f,o} - T_{amb} - \theta_1)}{T_{f,i} - T_{amb} - \theta_1} + (C_{p,0} + \alpha\theta_2) \ln \frac{\theta_2 - T_{f,i} + T_{amb}}{\theta_2 - T_{f,o} + T_{amb}} \right] \quad (4)$$

where,  $\theta_1$  and  $\theta_2$  are the arithmetical solutions of Eq. (5)  $\theta_1 < 0$ ,  $\theta_2 > 0$ .

$$\eta_o - a_1\theta - a_2\theta^2 = 0 \quad (5)$$

$$C_{p,a} = C_{p,0} + \alpha(T_{amb} - T_0) \quad (6)$$

Solar collectors' efficiency in the liquid phase can be computed by

$$\eta_{cl,l} = \frac{m_f(h_{l,o} - h_{l,i})}{GS_l} \quad (7)$$

Solar collectors' efficiency having organic fluid in the vapor phase and the thermal efficiency of the overall collector array is computed by Eqs. (8) and (10), respectively.

$$\eta_{cl,v} = \eta_{cl,0} - a_1(T_{evp} - T_{amb}) - a_2(T_{evp} - T_{amb})^2 \quad (8)$$

$$S_b = \frac{m_f(h_{b,o} - h_{b,i})}{G \times \eta_{cl,v}} \quad (9)$$

$$\eta_{cl} = \frac{m_f(h_{b,o} - h_{l,i})}{G(S_l + S_b)} \quad (10)$$

### 3.2. Thermal storage system

A heat storage tank filled with PCM is used in DVG solar ORC system as shown in Fig. 2. A shell and tube heat exchanger filled with PCM is employed. The cylindrical heat storage tank is filled with multiple tubes in it. Every big tube have a mini tube inside. The phase change material is filled in the tube having a larger diameter. However, organic fluid passes through the mini tube. Both of tubes are kept to equal length. However, the bigger tube has a 10 times larger diameter than mini-tube (Alvi et al., 2019). It is assumed that outside walls of the container and PCM tube are insulated. The heat storage tank works in charging and discharging mode based on operating and boundary conditions. Heat is delivered from working fluid to the PCM during charging mode. Conversely, PCM releases heat to the working fluid during the discharging mode.

Modeling of the PCM storage tank is carried out using the famous enthalpy method (Voller et al., 1987; Günther et al., 2009). Following assumptions have been made while developing the model to compute the flow of heat through heat storage tank.

- The conduction is a major mechanism to transfer heat within the PCM.
- One dimensional heat transmission is considered for the present study.
- Thermo-physical properties of the PCM remains constant during each phase.
- Natural convection can happen due to density difference is neglected in present model.

$$\rho \frac{\partial H}{\partial t} = \kappa_{pcm} \frac{\partial^2 T_{pcm}}{\partial y^2} \quad (11)$$

The sensible heat of the PCM can be computed by Eq. (12)

$$h(T) = \int_{T_m}^T \rho_{pcm} C_{pcm} dT_{pcm} \quad (12)$$

The total enthalpy of PCM is calculated by combining Eqs. (11) and (12), respectively.

$$B_{vH} = \begin{cases} \rho_{pcm} C_{pcm} (T_{pcm} - T_m) & \text{for } T_{pcm} < T_m \text{ Solid region} \\ \rho_{pcm} C_{pcm} (T_{pcm} - T_m) + \lambda \rho_{pcm} & \text{for } T_{pcm} > T_m \text{ Liquid region} \end{cases} \quad (13)$$

The Eq. (12) shows that if the PCM is lying in a solid region, it exclusively stores sensible heat. However, if the PCM lies in the liquid region, it stores both sensible and latent heat. The volumetric enthalpy of the PCM is used to derive the temperature

**Table 1**

Thermo-physical properties of the PCM employed in the present system (Agyenim et al., 2010).

Name of the PCM	MgCl <sub>2</sub> .6H <sub>2</sub> O	
PCM category	Inorganic	
Melting point temperature (°C)	116.7	
Latent heat (kJ/kg)	160	
Thermal conductivity (W/m <sup>2</sup> -°C)	Both states (solid & liquid)	0.7
Specific heat capacity (kJ/kg-°C)	Both states (solid & liquid)	2.61

of the PCM “T<sub>pcm</sub>” as presented in Eq. (14)

$$T_{pcm} = \begin{cases} T_m + \frac{H}{\rho_{pcm} \cdot C_{pcm}} & \text{for } T_{pcm} < T_m \text{ Solid region} \\ T_m & \text{for } T_{pcm} = T_m \text{ Marshy region} \\ T_m + \frac{H - (\rho_{pcm} \cdot \lambda)}{\rho_{pcm} \cdot C_{pcm}} & \text{for } T_{pcm} > T_m \text{ Liquid region} \end{cases} \quad (14)$$

where latent heat of the PCM is presented by λ the while ρ<sub>pcm</sub> depicts the density of PCM.

Furthermore, the quantity of heat stored by the PCM storage tank during charging process is computed by multiplying the total mass of the PCM “M<sub>pcm</sub>” with the difference in the maximum and minimum specific enthalpy of the PCM storage tank as depicted in Eq. (15)

$$Q_{st} = M_{pcm}(h_{mx} - h_{min}) \quad \text{for } T_{pcm} > T_m \text{ Liquid region} \quad (15)$$

Similarly, the quantity of heat released during the discharging process is computed by multiplying the difference in the maximum and minimum specific enthalpy of the PCM storage tank with the total mass of the PCM “M<sub>pcm</sub>” as shown in Eq. (16)

$$Q_{rel} = M_{pcm}(h_{mx} - h_{min}) \quad \text{for } T_{pcm} < T_m \text{ Solid region} \quad (16)$$

The total mass of PCM can be calculated by using Eq. (17)

$$M_{pcm} = \pi(r_{pcm}^2 - r_{fluid}^2) \times L_{pcm} \times \rho_{pcm} \quad (17)$$

where r is the radius, L is the length and ρ is the density, respectively. A commercially available, medium temperature PCM feasible for solar Organic Rankine cycle system is selected for this study (Manfrida et al., 2016; Alvi et al., 2019). Thermo-physical properties of the PCM employed in the present study are shown in Table 1.

### 3.3. Validation of the current model of the PCM

The experimental validation of the current numerical model is performed by comparing the experimental results of Lacroix (1993) with the numerical simulation results. The storage unit consisted of two concentric tubes having a diameter of 0.0127 m and 0.0258 m, respectively. Both of tubes had equal length of 1 m. The outside tube was well insulated. The space between tubes was filled with the PCM. The water was employed as HTF and circulated through the inner tube. The heat transfer fluid mass flow rate was kept at 0.0315 kg/s. The melting point temperature of the PCM (n-octadecane) used was 28.2 °C. To validate, the experimental results are reproduced using the present numerical simulation model. The results are reproduced for a case when HTF and PCM temperatures were taken at length of tube = 1.0. A good agreement is found in the experimental and numerical results as shown in Fig. 3. The thermo-physical properties of the n-octadecane PCM is listed in Table 2.

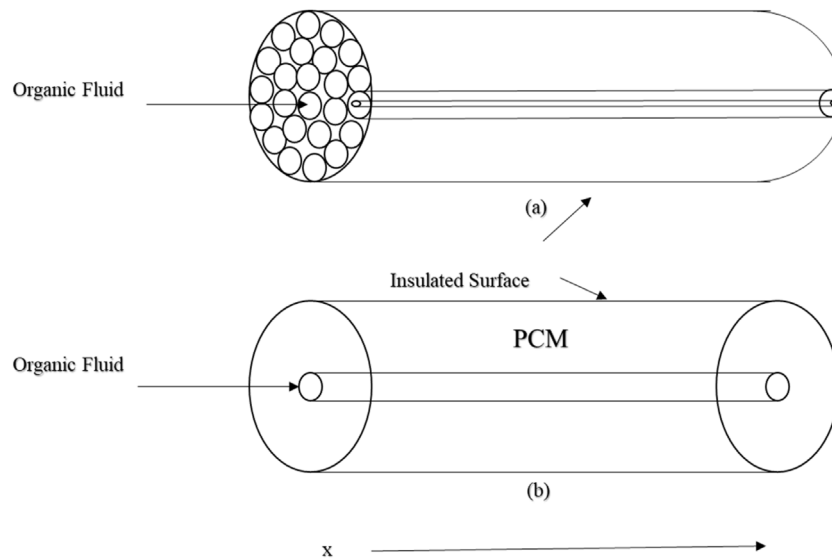


Fig. 2. A schematic diagram of the PCM storage tank.

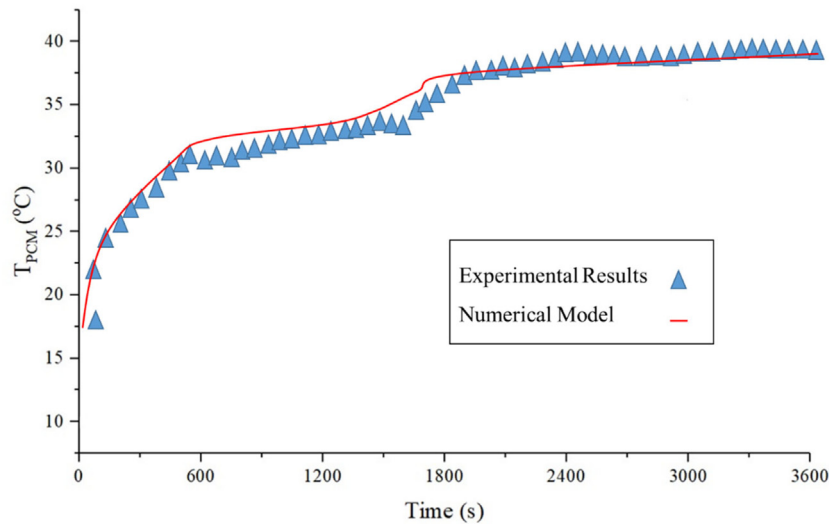


Fig. 3. The comparison of the results obtained by Lacroix (1993) with current numerical model.

**Table 2**  
Thermo-physical properties of Paraffin used by Lacroix (1993).

Melting point temperature (°C)		28.2
Latent heat (kJ/kg)		243.5
Density (kg/m <sup>3</sup> )	Solid	861
	Liquid	772
Thermal conductivity (W/m <sup>2</sup> -°C)	Solid	0.358
	Liquid	0.148
Specific heat capacity (kJ/kg-°C)	Solid	1.85
	Liquid	2.33

### 3.4. The basic Organic Rankine cycle

A basic organic Rankine cycle system is considered in this study because of its less complexity, low cost and suitability to low-medium temperature applications. Evaporation and condensation processes are assumed to be isobaric while expansion

**Table 3**  
The assumptions for the basic ORC.

Parameter	Value
Isentropic expander efficiency (Li et al., 2016c)	80%
Pump efficiency (Usman et al., 2017)	60%
Generator efficiency	85%
The condensation temperature	30 °C

and pressurization processes are adiabatic. Few presumption are made for operating conditions of the basic cycle as listed in Table 3.

The power produced by the expander and power used by the pump are evaluated by assessed by using Eqs. (18) and (19), respectively.

$$w_t = m_f(h_{t,i} - h_{t,o}) \tag{18}$$

$$w_p = m_f(h_{p,o} - h_{p,i}) \tag{19}$$

The isentropic efficiency of the expander and the pump are calculated by using Eqs. (20) and (21), respectively.

$$\varepsilon_t = \frac{h_{t,i} - h_{t,o}}{h_{t,i} - h_{t,os}} \quad (20)$$

$$\varepsilon_p = \frac{h_{p,os} - h_{p,i}}{h_{p,o} - h_{p,i}} \quad (21)$$

where the ideal thermodynamic process is presented by *os*. The quantity of energy utilized in the heating process of the ORC is computed by multiplying the mass flow rate of organic fluid with a rise in the enthalpy of working fluid from the pump to the expander.

$$q = m_f(h_{t,i} - h_{p,o}) \quad (22)$$

Finally, the ORC efficiency can be computed by dividing the net power output to the quantity of heat supplied, as shown in Eq. (23).

$$\eta_{ORC} = \frac{w_t \cdot \varepsilon_g - w_p}{q} \quad (23)$$

The overall system efficiency of the DVG solar ORC system can be computed by

$$\eta_{sys} = \eta_{ORC} \cdot \eta_{cl} \quad (24)$$

#### 4. Appropriate working fluid for DVG solar ORC system

There are different criteria to select appropriate working fluid for the solar ORC system such as thermodynamic efficiency, flammability, toxicity and other environmental factors (ODP and GWP), etc. (Delgado-Torres and García-Rodríguez, 2010). The working fluid selection for the solar ORC system is a challenging and crucial task. Moreover, it becomes more complicated for the DVG based solar ORC system because of its limitations such as the requirement of higher sensitivity to the environmental condition, higher operating pressure and temperature. The Refrprop 9.0 data base is used to select the appropriate working fluid (NSRD, 2010). Therefore, to meet all the needs, the working fluid should meet the following criteria's:

##### a. Slope on temperature entropy chart

The working fluids generally show three kinds of trends on the temperature-entropy *T-s* diagram. The first kind of working fluids that depicts a negative slope on the saturated vapor curve in the *T-s* diagram is called wet fluids. This kind of fluids requires to superheat at the entrance of the expander (Mago et al., 2008; Roy et al., 2011). Hence, wet fluids are not suitable for DVG solar ORC system because of the following reasons. Firstly, the thermal conductivity of the working fluids becomes very low at the superheated state. For example, the thermal conductivity of R1234ze(E) at an evaporation temperature of 150 °C and pressure of 2MPa (superheated state) is found to be 0.0247 W m<sup>-1</sup> K<sup>-1</sup>. Secondly, it is challenging to maintain the superheated state under the varying environmental conditions such as solar radiations, ambient temperature and wind speed, etc. Finally, it is also difficult for a PCM storage tank to work as a superheater under practical working conditions. Moreover, it requires a sophisticated control system to maintain the superheat for DVG solar ORC system.

The second and third kind of working fluids exhibits vertical and positive slope on the saturation vapor curve are called dry and isentropic fluid, respectively. These working fluids are preferred for DVG solar ORC system. Hence, they are selected in the present study because they do not require superheat before entering the expanders.

##### b. Thermal stability

In the case of the DVG solar ORC system, operating pressures and temperatures of working fluids are high. Therefore, thermal stability becomes an important parameter. Hence, the working fluids that are thermally stable up to a temperature of 200 °C and 4 MPa pressure are considered in this study (Li et al., 2016a).

##### c. Appropriate operating pressure

The DVG solar ORC system is comparatively more sensitive to operating pressure. Therefore, the operating pressure becomes a more critical parameter in the case of DVG based solar ORC system due to its higher operating pressure in comparison with the waste heat, biomass and geothermal ORC systems.

The technical demands like strength and cost of the solar thermal collectors, heat storage tank, piping system and other components become strict because of high operating pressure. Therefore, fluids having moderate evaporation pressure are preferred for DVG solar ORC system. Hence, the working fluids with evaporation pressure of less than 4 MPa at given operating conditions (bearable by solar collectors) are considered in this study (Li et al., 2016a).

##### d. Suitable critical temperature

In the practical operation of the supercritical DVG solar ORC system, it is tough to manage the temperature and pressure at the outlet of solar collector array. Moreover, it can affect the off-design performance of the expander. Therefore, the supercritical cycle is not feasible for DVG solar ORC system.

However, in a subcritical cycle, a PCM storage tank can be used to achieve a constant temperature and pressure at expander inlet. Moreover, In Fig. 1 system is designed to operate at charging and discharging mode. Therefore, the working fluids having a critical temperature higher than the given evaporation temperature are considered in this study.

##### e. Environmental factors

The ozone depletion potential (ODP) and global warming potential (GWP) are the factors that present working fluid impact on the environment. The working having low values of ODP and GWP are considered to be suitable for the solar ORC system. Hence, the fluids having ODP = 0 and GWP ≤ 1000 are considered in this study.

Some other factors such as toxicity and flammability etc. can also be important during selection process but they are not considered in the present study. Because, the working fluid selection is a complex process and one cannot find a fluid which fulfills all criteria's. Hence, it is the trade-off between different parameters. Therefore, various working fluids are selected depending upon their application, operating and boundary conditions. Properties and system efficiencies of working fluids chosen based on the above-mentioned criteria's in the present study are listed in Table 4.

#### 5. Results and discussions

In this part, the impact of the working fluids on the working of the PCM based DVG solar ORC system concerning their critical point temperature is evaluated and compared during the charging and discharging process, respectively. The variation in the overall system efficiency at a given evaporation temperature of working fluid, mass flow rate of working fluid and length of PCM tube are analyzed and discussed. Moreover, the impact of critical point temperature of working fluid on rise and fall of organic fluid temperature, PCM temperature and the quantity of energy stored and released during charging and discharging mode is also investigated. A time step of 1 h is chosen to carry out whole simulation process. The average temperature of PCM and working

**Table 4**  
Working fluids properties and their system efficiencies at different levels of evaporation temperature.

Working fluid	T <sub>c</sub> (°C)	P <sub>c</sub> (bar)	ODP	GWP	System efficiency at different levels of evaporation temperature (%)					
					T <sub>evp</sub> = T <sub>m</sub> + 10 °C	T <sub>evp</sub> = T <sub>m</sub> + 20 °C	T <sub>evp</sub> = T <sub>m</sub> + 30 °C	T <sub>evp</sub> = T <sub>m</sub> - 10 °C	T <sub>evp</sub> = T <sub>m</sub> - 20 °C	T <sub>evp</sub> = T <sub>m</sub> - 30 °C
Benzene	288.87	49.7	0	0	10.7	10.9	11.1	10.4	10.3	10.2
Cyclohexane	280.45	40.81	0	0	10.3	10.4	10.6	9.97	9.87	9.81
Heptane	266.98	27.36	0	0	9.72	9.85	9.97	9.5	9.43	9.4
Hexane	234.68	30.34	0	0	9.71	9.87	10	9.35	9.18	9.05
Isohexane	224.55	30.4	0	0	9.51	9.66	9.77	9.17	9	8.87
Pentane	196.55	33.7	0	0	9.52	9.63	9.63	9.13	8.89	8.65
Isopentane	187.2	33.78	0	4	9.23	9.27	9.15	8.9	8.67	8.43
R245ca	174.42	39.25	0	693	9.49	9.39	8.87	9.15	8.85	8.51
RE245fa2	171.73	34.33	0	812	9.4	9.31	8.77	9	8.67	8.3
R1233zd(E)	165.6	35.73	0	1	9.34	9	7.96	9.11	8.79	8.4
R245fa	154.01	36.51	0	858	8.1	7.11	4.53	8.4	8.21	7.9
Butane	151.98	37.96	0	4	7.83	6.63	3.44	8.32	8.19	7.94

fluid during 1 h time period is used and presented in the current study.

*5.1. Performance evaluation of the phase change material based DVG solar ORC system at given evaporation temperature*

A basic subcritical DVG solar ORC is considered in this study. The performance of the solar ORC system is evaluated at different levels of evaporation temperature. The evaporation temperature is kept 10 °C, 20 °C and 30 °C higher and lower than PCM melting point temperature to keep the system under charging and discharging mode, respectively. The mass flow rate of working fluid is kept 1 kg/s and the length of the PCM tube is kept 36 m.

*5.1.1. Impact of critical point temperature of the working fluid on system efficiency at given evaporation temperature*

The overall performance of the solar ORC system is depicted by system efficiency. It is a multiple of ORC and collector efficiency. The change in system efficiency concerning the critical point temperature of the working fluid at a given evaporation temperature is shown in Fig. 4. The overall system efficiency generally increases with an increase in the critical temperature of the working fluid during charging and discharging mode, respectively.

Working fluids having lower critical point temperatures have shown higher decrement in the system efficiency in comparison with higher critical temperature working fluids with an increase and decrease in evaporation temperature during charging and discharging mode, respectively. For instance, Butane has shown a maximum decrease in system efficiency of 4.38% and 0.38% with a 20 °C increase and decrease in evaporation temperature while Benzene has shown the least decrement of 0.19% and 0.18% during charging and discharging mode, respectively. This can happen because of the high evaporation temperature during the charging mode. The heat collection efficiency or collector efficiency decreases drastically when evaporation temperature becomes closer to the critical temperature of the working fluid. Hence, it further impacts the overall system efficiency.

At a given evaporation temperature, the relative increment in system efficiency is higher during charging mode than discharging mode. For example, at an evaporation temperature of T<sub>m</sub>+30 °C, the system efficiency of Benzene is found to be 7.69% higher than Butane. However, its value becomes 2.38% at an evaporation temperature of T<sub>m</sub>-30 °C. Conclusively, working fluids having higher critical temperature have shown overall better performance by achieving higher system efficiencies.

*5.1.2. Impact of critical temperature on the rise and fall in the temperature of working fluid within the PCM storage tank at a given evaporation temperature*

The variation in working fluid temperature within the PCM storage tank gives the idea of heat transfer between working fluid and PCM. Therefore, it can help the engineers to select the suitable working fluid for PCM based DVG solar system. The working fluid temperature increase and decrease during charging and discharging mode, respectively. The variation in working fluid temperature within the PCM storage tank at a given evaporation temperature is shown in Fig. 5. The rise and fall in working fluid temperature generally increase with an increase in critical temperature.

The working fluids having higher critical point temperatures have shown the higher increment in rise and fall of working fluid temperature with an increase in evaporation temperature while working fluids having lower critical point temperatures have shown minimum increment. For example, Heptane has shown maximum increment in rise and fall in working fluid temperature of 9.49 °C and 16.28 °C with a 20 °C increase in evaporation temperature while R245fa has shown a minimum increment of 0.89 °C and 6.5 °C during charging and discharging mode, respectively.

At a given evaporation temperature, the relative increment in the rise of working fluids temperatures is higher during discharging mode as compared to fall in working fluids temperatures during charging mode. For example, at the evaporation temperature of T<sub>m</sub>-10 °C, the rise in temperature of Heptane within the PCM storage tank is 13.48 °C higher than the rise in temperature of R245fa.

However, at the evaporation temperature of T<sub>m</sub>+10 °C, the fall in temperature of Heptane within the PCM storage tank is only 3.78 °C higher than the fall in temperature of R245fa. Finally, working fluids having higher critical temperatures have shown overall better performance in terms of higher rise and fall in working fluids temperatures.

*5.1.3. Impact of critical temperature on the rise and fall in the PCM temperature at a given evaporation temperature*

The PCM temperature gives an idea about the heat stored and released by the PCM during charging and discharge mode. The temperature of the PCM decrease and increase during charging and discharging mode, respectively. The variation in working fluid temperature within the PCM at a given evaporation temperature is shown in Fig. 6.

The rise and fall in PCM temperature generally increase with an increase in critical temperature. In contrast to working fluid temperature, rise and fall in PCM temperature is much lesser.

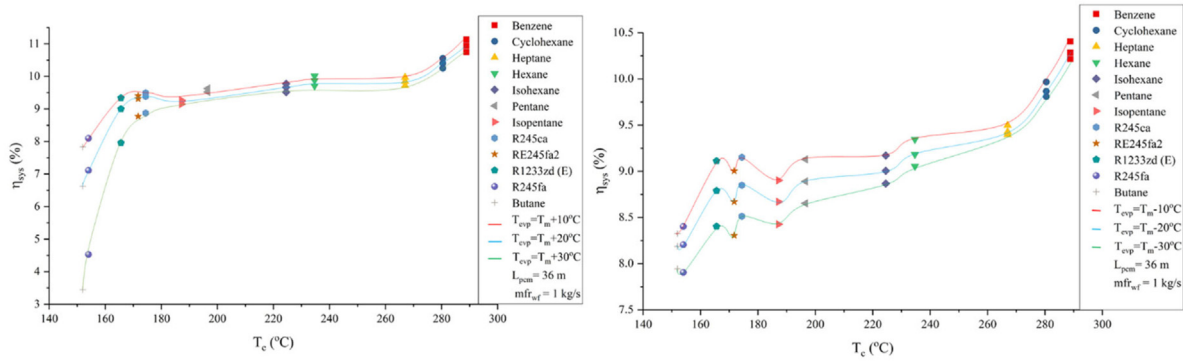


Fig. 4. Impact of critical point temperature of working fluids on the system efficiency, left: Charging mode, right: Discharging mode.

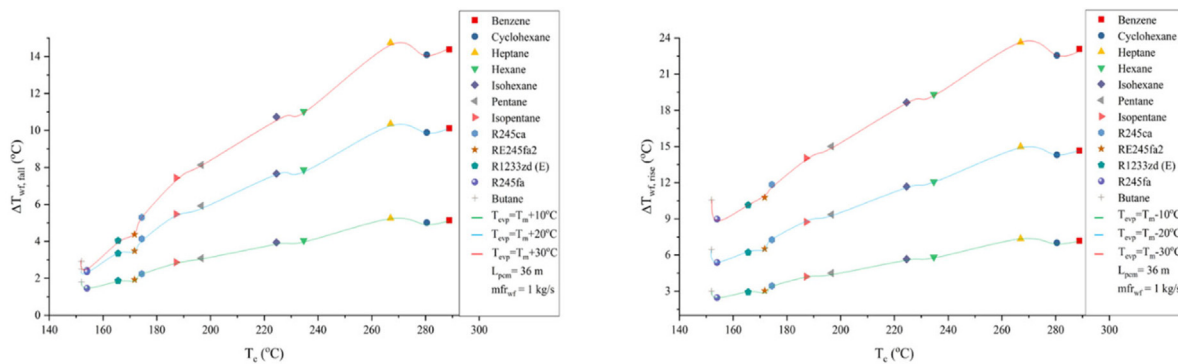


Fig. 5. Impact of critical point temperature of working fluids on The variation in working fluid temperature with in the PCM storage tank, left: Charging mode, right: Discharging mode.

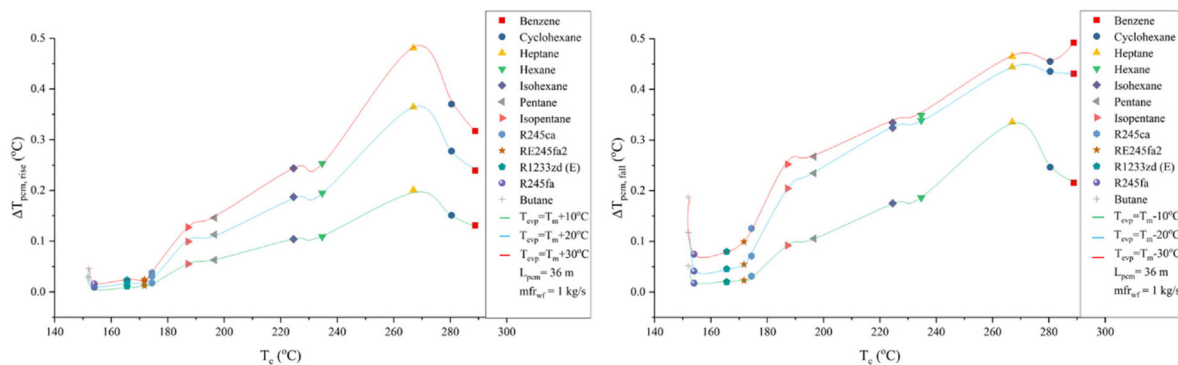


Fig. 6. Impact of critical point temperature of working fluids on The variation in PCM temperature, left: Charging mode, right: Discharging mode.

However, the working fluids having higher critical point temperatures have shown the higher increment in rise and fall of PCM temperature with an increase in evaporation temperature while working fluids having lower critical point temperatures have shown lesser increment. For instance, Heptane and Benzene have shown maximum rise and fall in temperature of the PCM of 0.28 °C and 0.27 °C with an increase in evaporation temperature of 20 °C during charging and discharging mode, respectively. However, R1233zd(E) and R245fa has depicted the negligible rise and fall in temperature of the PCM of 0.07 °C and 0.06 °C with an increase in evaporation temperature of 20 °C during charging and discharging mode, respectively.

Moreover, at a given evaporation temperature, the relative increment in rise and fall in PCM temperature is higher during discharging as compared to charging mode. For example, at evaporation temperature of  $T_m + 10$  °C, the average temperature of

PCM using Heptane as working fluid is 0.19 °C higher than the average temperature of PCM using R25fa as working fluid.

However, at evaporation temperature of  $T_m - 10$  °C, the average temperature of PCM using Heptane as working fluid is only 0.3 °C higher than average temperature PCM using R25fa as working fluid. Finally, Benzene and Heptane have shown better performance because of the higher rise and fall in PCM temperatures.

#### 5.1.4. Impact of critical temperature on the quantity of energy stored and released by the PCM at a given evaporation temperature

The quantity of energy stored and released is one of the core criteria to analyze the performance of PCM storage. It can be computed by multiplying the change in latent heat of PCM with a mass of PCM. It generally increases with an increase in the critical temperature of the working fluid. Fig. 7 represents the impact of critical point temperature of working fluid on the quantity of

heat stored and released by PCM during charging and discharging mode, respectively.

The working fluids having higher critical point temperatures have shown a higher increment in the quantity of energy stored and released by the PCM with an increase in evaporation temperature while working fluids having lower critical point temperatures have shown lower increment. For example, Heptane depicts the maximum increase in the quantity of energy stored and released of 19.36 MJ and 71.05 MJ with an increase of 20 °C in evaporation temperature while R245fa has shown a minimum increase of 0.46 MJ and 4 MJ during charging and discharging mode, respectively.

The quantity of energy stored by PCMs during the charging mode is lower than the energy released in discharging mode at a given evaporation temperature. For instance, at an evaporation temperature of  $T_m \pm 30$  °C, the quantity of energy released by PCM during discharging mode while using Heptane as working fluid is found to be 60.92 MJ more than the quantity of energy stored by PCM during charging mode.

Conclusively, working fluids with higher critical temperatures have shown better performance in terms of the quantity of energy stored and released by the PCM.

## 5.2. Performance evaluation of the phased change material based DVG solar ORC system at given mass flow rate

Mass flow rate is another parameter that significantly impacts the performance of the solar ORC system.

The performance of the system is evaluated at different levels of the mass flow rate of the organic fluid. The mass flow rate of organic fluid is kept 0.5, 0.75 and 1 kg/s during charging and discharging mode, respectively. The evaporation temperature is kept 10 °C higher and lower than PCM melting point temperature to keep the system under charging and discharging mode, respectively.

### 5.2.1. Impact of critical point temperature of working fluid on system efficiency at given mass flow rate

Mass flow rate of working fluid significantly impacts the system efficiency of PCM based DVG solar ORC system. The impact of the critical point temperature of the working fluids on overall system efficiency at a given mass flow rate of organic fluid is shown in Fig. 8. The system efficiency increase in the beginning, becomes consistent in the middle and increase in the end concerning critical temperature working fluids.

The working fluids having higher critical point temperatures have shown higher increment in the system efficiency with an increase in mass flow rate as compared to the working fluids having lower critical point temperatures. For example, the system efficiency of Benzene increases by 5.39% and 5.17% with 0.5 kg/s increase in the mass flow rate of working fluid during charging and discharging mode, respectively. While, the system efficiency of Butane increase by 3.92% and 4.15% with 0.5 kg/s increase in mass flow rate of working fluid during charging and discharging mode, respectively.

Relative increment in system efficiency increases with an increase in mass flow rate of the working fluid. For example, at mass flow rate of 0.5 kg/s, the difference in system efficiency of Benzene and Butane is found to be 1.4% and 1.05% during charging and discharging mode, respectively. However, at the mass flow rate of 1 kg/s, its value becomes 2.91% and 2.01% during charging and discharging mode, respectively.

Conclusively, working fluids with higher critical temperatures have shown better performance in terms of higher system efficiencies.

### 5.2.2. Impact of critical temperature on the rise and fall in the temperature of working fluid within the PCM storage tank at a given mass flow rate

The rise and fall in organic fluid temperature while passing through a PCM storage tank is an important parameter to measure the performance of a heat storage tank, which further impacts overall system performance. The impact of critical point temperature of working fluid on the rise and fall in working fluid temperature at a given mass flow rate is shown in Fig. 9. The rise and fall in working fluid temperature generally increase with an increase in the critical point temperature of the working fluid.

Working fluids having higher critical point temperatures have shown larger increment in the rise and fall of organic fluid temperature with an increase in mass flow rate while working fluids of low critical point temperatures have shown lesser decrement. For example, Heptane has shown a larger increment of 0.49 °C and 0.6 °C with a 0.5 kg/s increase in mass flow rate while Butane has shown a lesser increment of 0.25 °C and 0.39 °C during charging and discharging mode, respectively.

At a given mass flow rate, the relative increment in fall of working fluid temperature is higher than the rise during discharging as compared to the charging mode. For example, at a mass flow rate of 0.5 kg/s during charging mode, the rise in temperature of Heptane within PCM storage tank is 4.10 °C higher than rise in temperature of R25fa. However, during discharging mode, the fall in temperature of Heptane within PCM storage tank is 5.18 °C higher than fall in temperature of R25fa.

Conclusively, working fluids having higher critical temperatures have shown overall better performance because of their higher rise and fall in working fluids temperatures.

### 5.2.3. Impact of critical temperature on the rise and fall in the PCM temperature at a given mass flow rate

The variation in mass flow rate can impact the PCM temperature, which can further impact the heat storage performance. The effect of critical point temperature of working fluid on rise and fall in PCM temperature at a given mass flow rate is shown in Fig. 10. The rise and fall in PCM temperature generally increase with an increase in the critical point temperature of the working fluid.

The rise and fall in PCM temperature is much lesser as compared to working fluid temperature. The working fluids having higher critical point temperatures have shown the maximum increment in the rise and fall of PCM temperature with an increase in mass flow rate while working fluids having lower critical point temperatures have shown minimum or no increment. For instance, Heptane has shown maximum rise and fall in temperature of the PCM of 0.07 °C and 0.12 °C with an increase in the mass flow rate of 0.5 kg/s during charging and discharging mode, respectively. However, R245fa has depicted the no rise and fall in temperature of the PCM with an increase in mass flow rate of 0.5 kg/s during charging and discharging mode, respectively. Finally, Heptane has shown better performance because of higher rise and fall in PCM temperatures.

### 5.2.4. Impact of critical temperature on the quantity of energy stored and released by the PCM at a given mass flow rate

The quantity of energy stored and released are the major criteria to evaluate the performance of a heat storage tank. Therefore, Fig. 11 depicts the impact of the critical point temperature of working fluid on the quantity of energy stored and released during charging and discharging mode at a given mass flow rate. The quantity of energy stored and released generally increases with an increase in the critical point temperature of the working fluid.

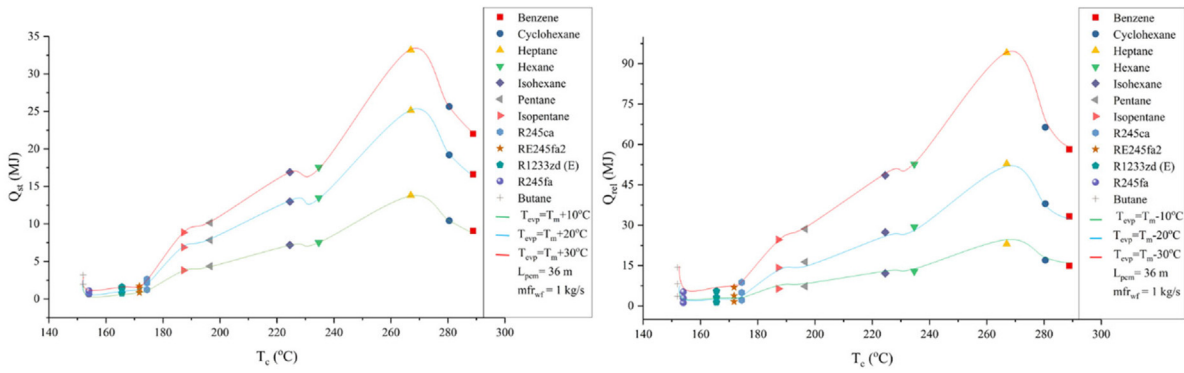


Fig. 7. Impact of critical point temperature of working fluids on the quantity of energy stored and released by PCM, left: Charging mode, right: Discharging mode.

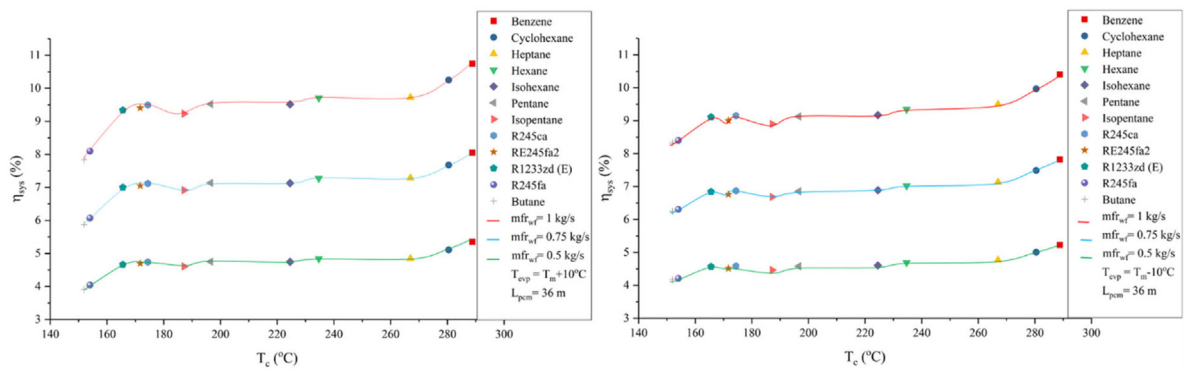


Fig. 8. Impact of critical point temperature of working fluids on the system efficiency, left: Charging mode, right: Discharging mode.

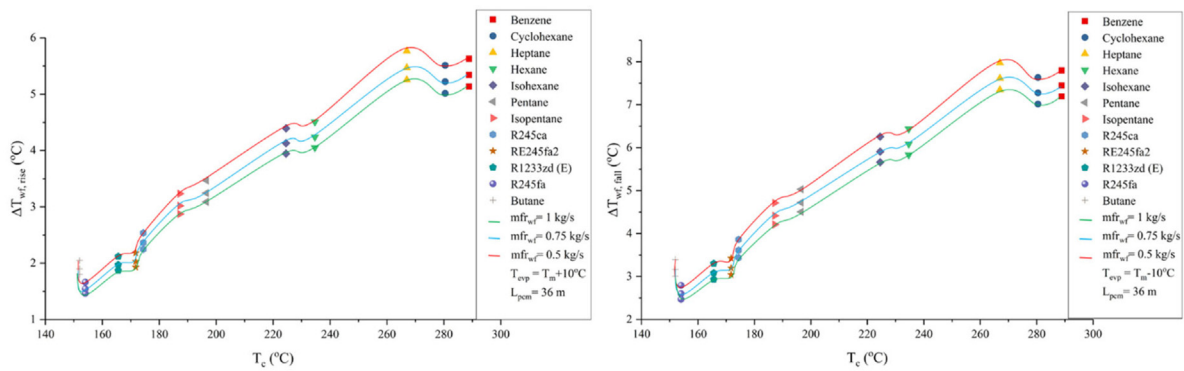


Fig. 9. Impact of critical point temperature of working fluids on The variation in working fluid temperature within the PCM storage tank, left: Charging mode, right: Discharging mode.

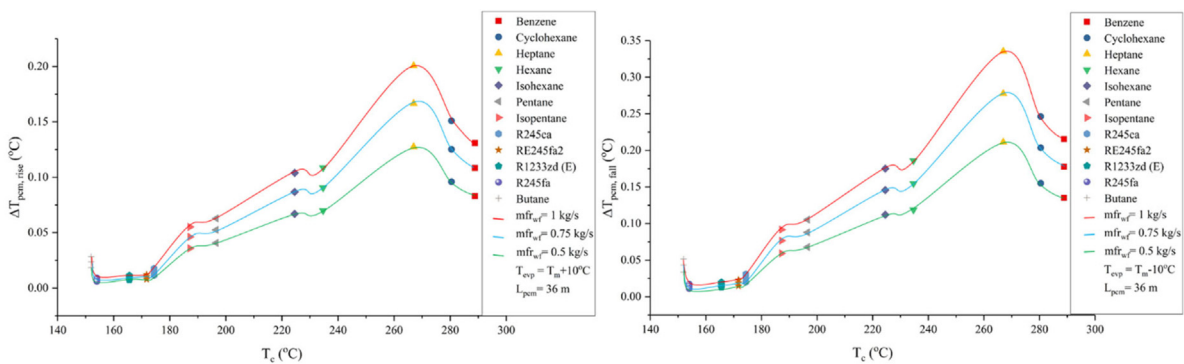


Fig. 10. Impact of critical point temperature of working fluids on The variation in PCM temperature, left Charging mode, right: Discharging mode.

The working fluids having higher critical point temperatures have shown the higher increment in the quantity of energy stored and released by the PCM with an increase in mass flow rate while working fluids having lower critical point temperatures have shown lower increment. For example, Heptane depicts the maximum increase in the quantity of energy stored and released of 4.9 MJ and 8.38 MJ with an increase of 0.5 kg/s in evaporation temperature while R245fa has shown a minimum increase of 0.22 MJ and 0.42 MJ during charging and discharging mode, respectively.

Conclusively, working fluids with higher critical temperature have shown better performance in terms of quantity of energy stored and released by the PCM.

### 5.3. Performance evaluation of the phase change material based DVG solar ORC system at a given length of PCM tube

The length of PCM tube is another parameter that significantly impacts the performance of the phase change material based DVG solar ORC system. The working of the system is evaluated at different lengths of the PCM tube. The length of PCM tube is kept 36, 48 and 72 m during charging and discharging mode, respectively. The evaporation temperature is kept 10 °C higher and lower than PCM melting point temperature to keep the system under charging and discharging mode, respectively. Moreover, the mass flow rate is kept 1 kg/s.

#### 5.3.1. Impact of critical point temperature of working fluid on system efficiency at a given length of PCM tube

The length of PCM tube is the parameter that directly affects the size of the heat storage tank. Therefore, it significantly affects the performance of heat storage. However, it does not significantly impact the overall system efficiency. The impact of the critical point temperature of the working fluids on overall system efficiency at a given length of PCM tube is shown in Fig. 12.

The overall system efficiency generally increases with an increase in the critical temperature of the working fluid during charging and discharging mode, respectively. The system efficiency does not significantly improve by increasing the length of PCM tube. For example, the system efficiency of Benzene merely increases by 0.23% and 0.27% with a 36 m increase in the length of the PCM tube during charging and discharging mode. Moreover, working fluids having higher critical temperatures have shown overall better performance by achieving higher system efficiencies.

#### 5.3.2. Impact of critical temperature on the rise and fall in the temperature of working fluid within the PCM storage tank at a given length of PCM tube

Rise and fall in working fluid temperature can significantly affect by varying the length PCM tube. It increases and decreases with increment and decrement in the length of PCM tube. Fig. 13 shows the effect critical temperature of the working fluid on the rise and fall of working fluid temperature within the PCM tube at a given length of PCM tube. The rise and fall of working fluid temperature is found to be an increasing function of the critical temperature of working fluid.

Working fluids have shown a similar increment in the rise and fall of organic fluid temperature with an increase in the critical point temperature of working fluids. For example, Heptane has shown a similar increment of 3.09 °C and 3.25 °C with a 36 m increase in length of PCM tube. Similarly, Butane has shown an almost equal increment of 3.25 °C and 3.79 °C during charging and discharging mode, respectively.

At a given length of PCM tube, the relative increment in rising and fall of working fluid temperature is higher during discharging

as compared to charging mode. For example, at 72 m length of PCM tube during charging mode, the average temperature of Heptane within the PCM storage tank is 4.63 °C higher than the average temperature of R25fa. However, during discharging mode, the average temperature of Heptane within PCM storage tank is only 4.72 °C higher than the average temperature of R25fa.

Conclusively, working fluids having higher critical temperature have shown overall better performance because of their higher rise and fall in working fluids temperatures.

#### 5.3.3. Impact of critical temperature on the rise and fall in the PCM temperature at a given length of PCM tube

The temperature of the PCM can determine the working of heat storage. The change in the temperature of PCM with a critical temperature of working fluid is shown in Fig. 14. The rise and fall in PCM temperature increase with an increase in the critical temperature of the working fluid.

The working fluids having higher critical point temperatures have shown the maximum increment in the rise and fall of PCM temperature with an increase in the length of PCM tube while working fluids having lower critical point temperatures have shown minimum or no increment. For instance, Heptane has shown maximum rise and fall in temperature of the PCM of 0.12 °C and 0.15 °C with an increase in the length of PCM tube by 36 m during charging and discharging mode, respectively. However, R245fa has depicted the negligible rise and fall in temperature of the PCM with an increase in the length of PCM tube by 36 m during charging and discharging mode, respectively. Finally, Heptane has shown better performance because of the higher rise and fall in PCM temperatures.

#### 5.3.4. Impact of critical temperature on the quantity of energy stored and released by the PCM at a given length of PCM tube

The quantity of energy stored and released can be affected by length of PCM tube. The impact of the critical point temperature of working fluid on the quantity of energy stored and released during charging and discharging mode at a given length of PCM tube is shown in Fig. 15. The quantity of energy stored and released generally increases with an increase in critical point temperature of the working fluid.

The working fluids having higher critical point temperatures have shown a higher increment in the quantity of energy stored and released by the PCM with an increase in the length of PCM tube while working fluids having lower critical point temperatures have shown lower increment. For example, Heptane depicts the maximum increase in the quantity of energy stored and released of 53.02 MJ and 77.98 MJ with an increase of 36 m in the length of the PCM tube while R245fa has shown a minimum increase of 4.32 MJ and 7.62 MJ during charging and discharging mode, respectively.

Conclusively, working fluids with higher critical temperatures have shown better performance in terms of the quantity of energy stored and released by the PCM.

## 6. Conclusions

A Phase change material based direct vapor generation solar ORC system is considered in this study. An array of evacuated flat plate collectors is used to transmit heat to the system. The PCM storage tank is coupled with the system for the stability of power generation. Moreover, 12 different working fluids are employed to evaluate the overall performance of the system. The whole system is modeled in MATLAB program to simulate charging and discharging mode. The simulation period is kept 1 h during both modes for each PCM employed in the system.

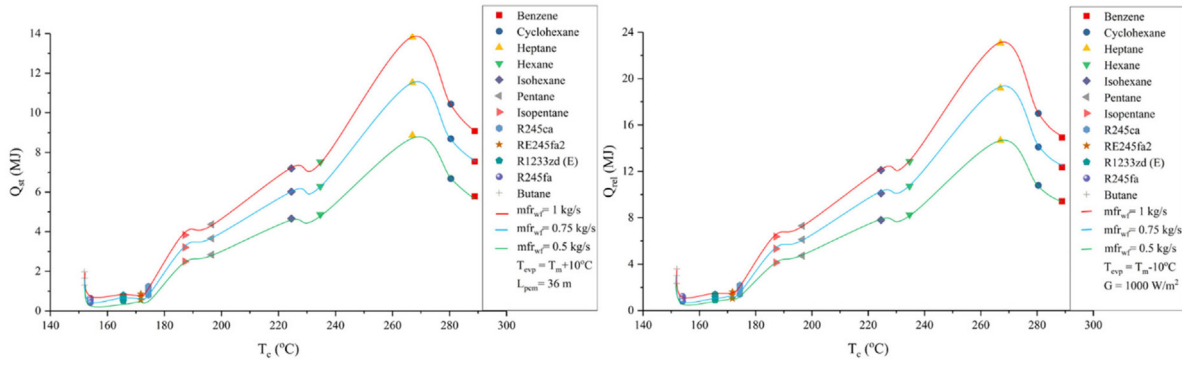


Fig. 11. Impact of critical point temperature of working fluids on The quantity of energy stored and released by PCM, left: Charging mode, right: Discharging mode.

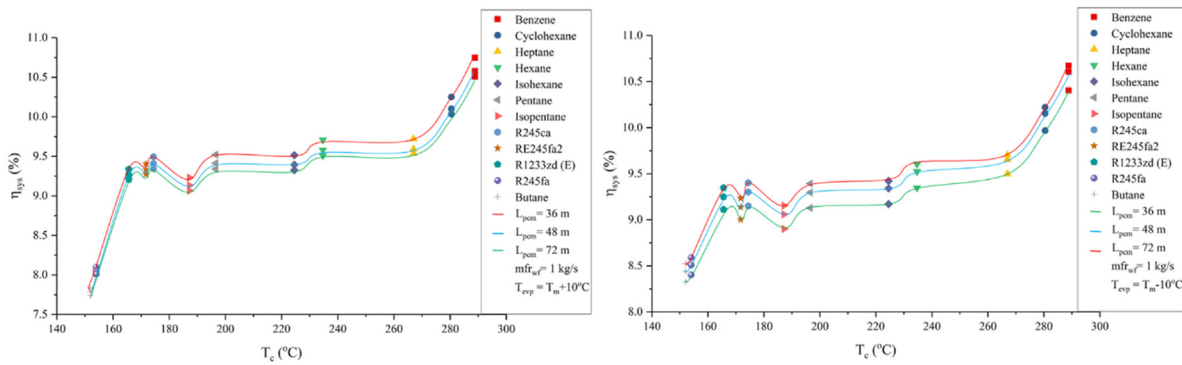


Fig. 12. Impact of critical point temperature of working fluids on system efficiency, left: Charging mode, right: Discharging mode.

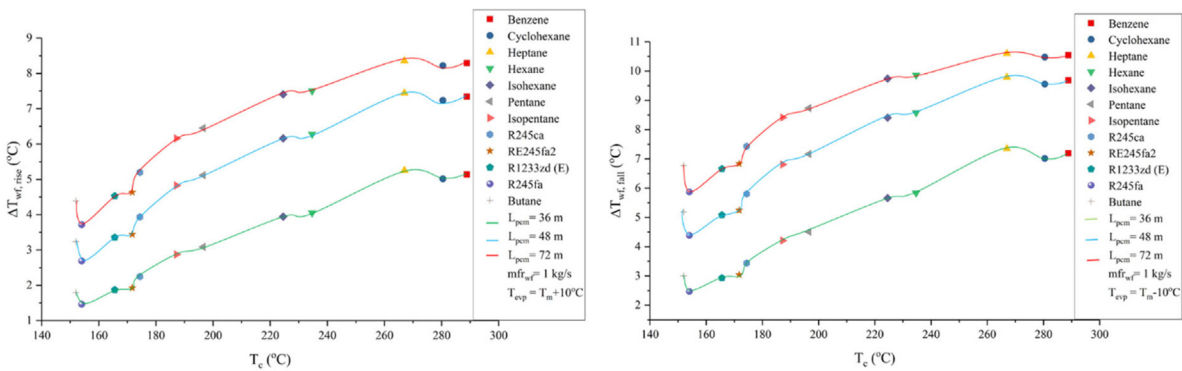


Fig. 13. Impact of critical point temperature of working fluids on The variation in working fluid temperature within the PCM storage tank, left: Charging mode, right: Discharging mode.

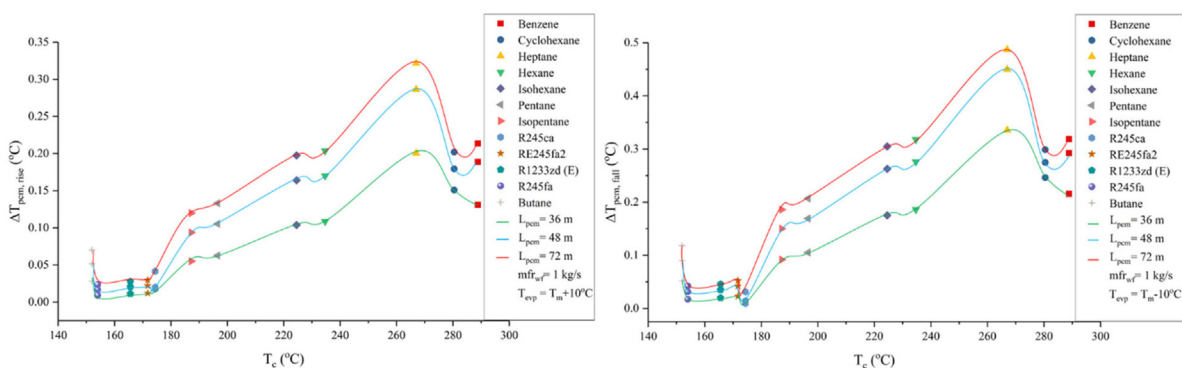


Fig. 14. Impact of critical point temperature of working fluids on The variation in PCM temperature, left: Charging mode, right: Discharging mode.

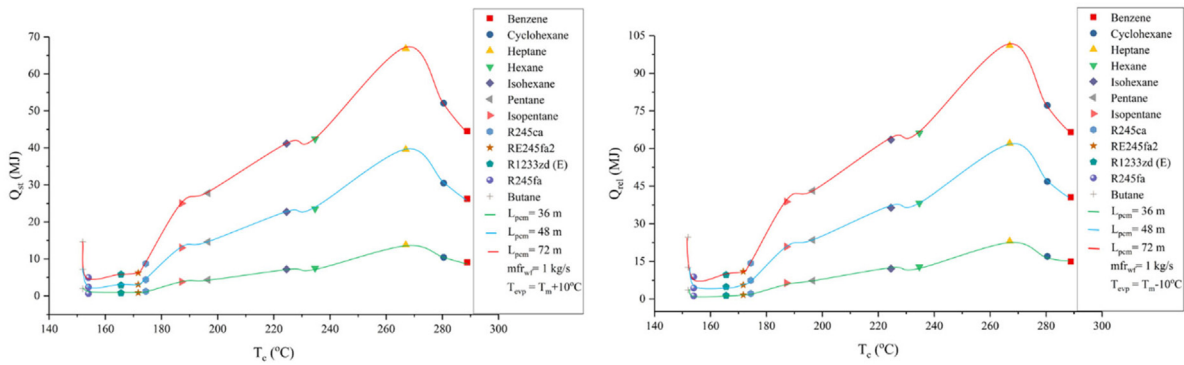


Fig. 15. Impact of critical point temperature of working fluids on The quantity of energy stored and released by PCM, left: Charging mode, right: Discharging mode.

The impact of evaporation temperature and mass flow rate and length of PCM tube on ORC, collector and overall system efficiency is analyzed during charging and discharging mode. At given operating conditions, working fluids having a higher critical point temperature have shown higher ORC efficiency. Conversely, the collector efficiency is higher for the working fluids having low critical point temperature. However, the working fluids having high critical point temperature have shown better performance in terms of overall system efficiency. For example, at given evaporation temperature, mass flow rate and length of PCM tube, Benzene has achieved maximum system efficiency during both modes of operation. However, MgCl<sub>2</sub>.6H<sub>2</sub>O has shown the highest overall system efficiency at given evaporation temperature and mass flow rate during both modes of the operation. Moreover, ORC efficiency is found to be in the range of 9% to 16%, the collector efficiency lies between 16% to 62% and overall system efficiency remains in 2% to 7.5% during both modes of operation.

The effect of evaporation temperature, mass flow rate and length of PCM tube on variation in working fluid temperature, PCM temperature and quantity of energy stored and released during charging and discharging mode is also evaluated. At given evaporation temperature, mass flow rate and length of PCM tube, the working fluids having a higher critical point temperature have shown higher working fluid temperature, PCM temperature and quantity of energy stored and released during charging and discharging mode, respectively. Finally, heptane has shown best performance among the selected fluids in terms of working fluid temperature, PCM temperature and quantity of energy stored and released during charging and discharging mode, respectively.

The present study only consider performance of the PCM based DVG solar ORC system during 1 h time period. However, the dynamic response is essential to ensure the continuous operation of the system, which require the development of dynamic model of PCM as well as the ORC system at component level. Authors are interested to explore the dynamic response and control of the system to ensure its continuous operation in their future work.

**Nomenclature**

*Symbols*

$w_t$	Work done by expander (W)
$w_p$	Work done by pump (W)
$h_{t,i}$	Enthalpy at expander inlet (kJ/kg)
$h_{t,o}$	Enthalpy at expander outlet (kJ/kg)
$h_{t,os}$	Enthalpy of expander at ideal thermodynamic process (kJ/kg)
$m$	Working fluid mass flow rate (kg/s)
$\epsilon_t$	Efficiency of expander (%)
$\epsilon_p$	Efficiency of pump (%)

$\eta_{ORC}$	Efficiency of organic Rankine cycle (%)
A	Area (m <sup>2</sup> )
G	Irradiation (W/m <sup>2</sup> )
T	Temperature of collector (°C)
T <sub>c</sub>	Critical temperature (°C)
T <sub>a</sub>	Ambient temperature (°C)
c <sub>p</sub>	Specific heat (J/(kg K))
λ	Latent heat of the PCM (J/kg)
$xT_{f,o}$	Temperature of fluid at collector outlet (°C)
$T_{f,i}$	Temperature of fluid at collector inlet (°C)
S <sub>l</sub>	Surface area of collector in liquid phase (m <sup>2</sup> )
S <sub>b</sub>	Surface area of collector in binary phase (m <sup>2</sup> )
$\eta_{c,l}$	Efficiency of collector in liquid phase (%)
$\eta_{c,v}$	Efficiency of collector in binary phase (%)
$h_{l,o}$	Enthalpy at liquid phase outlet (kJ/kg)
$h_{l,i}$	Enthalpy at liquid phase inlet (kJ/kg)
$h_{b,o}$	Enthalpy at binary phase outlet (kJ/kg)
$h_{b,i}$	Enthalpy at binary phase inlet (kJ/kg)
$m_f$	Working fluid mass flow rate (kg/s)
$\eta_c$	Efficiency of collector system (%)
$\eta_o$	Maximum Efficiency (%)
$\eta_{sys}$	System thermal efficiency (%)
$\epsilon_g$	Generator efficiency (%)
ρ	Density (g/m <sup>3</sup> )
<b>Abbreviations</b>	
GWP	Global Warming Potential
ODP	Ozone Depletion Potential
ORC	Organic Rankine Cycle
DVG	Direct vapor generation
FPC	Flat plate collector
CPC	Compound parabolic concentrator
ETC	Evacuated tube collector
PTC	Parabolic trough concentrator
CHP	Combined heat and power
HTF	Heat transfer fluid
DSG	direct steam generation
CSP	Concentrated solar power
PCM	Phase change material
G	Generator
P	Pump
<b>Subscript</b>	
ORC	Organic Rankine Cycle
Opt	Optimum
max	Maximum
Sys	System
c	Critical
i	Inlet

o	Outlet
O	Reference state
m	Melting point
evp	Evaporation

## Declaration of competing interest

The authors declare that they have no known competing financial interests or personal relationships that could have appeared to influence the work reported in this paper.

## Acknowledgments

This research work has been supported by the National Natural Science Foundation of China (51806081 and 51876083), the Natural Science Foundation of Jiangsu Province, China (BK20180882), the Key Research and Development Program of Jiangsu Province, China (BE2019009-4), the Natural Science Foundation of Jiangsu Province, China (BK20180882), the Key Research and Development Program of Zhenjiang City, China (SH2019008), and the Key Project of Taizhou New Energy Research Institute, Jiangsu University, China (2018–20).

## References

- Agyenim, F., Hewitt, N., Eames, P., Smyth, M., 2010. A review of materials, heat transfer and phase change problem formulation for latent heat thermal energy storage systems (LHTES). *Renew. Sustain. Energy Rev.* 14, 615–628. <http://dx.doi.org/10.1016/j.rser.2009.10.015>.
- Alvi, J.Z., Feng, Y., Wang, Q., Imran, M., 2019. Modelling, simulation and comparison of phase change material storage. *Appl. Therm. Eng.* 114780. <http://dx.doi.org/10.1016/j.applthermaleng.2019.114780>.
- Alvi, J.Z., Imran, M., Pei, G., Li, J., Gao, G., Alvi, J., 2017. Thermodynamic comparison and dynamic simulation of direct and indirect solar organic Rankine cycle systems with PCM storage. *Energy Procedia* 129, 716–723. <http://dx.doi.org/10.1016/j.egypro.2017.09.103>.
- Bu, X.B., Li, H.S., Wang, L.B., 2013. Performance analysis and working fluids selection of solar powered organic Rankine-vapor compression ice maker. *Sol. Energy* 95, 271–278. <http://dx.doi.org/10.1016/j.solener.2013.06.024>.
- Calise, F., D'Accadia, M.D., Vicidomini, M., Scarpellino, M., 2015. Design and simulation of a prototype of a small-scale solar CHP system based on evacuated flat-plate solar collectors and Organic Rankine Cycle. *Energy Convers. Manage.* 90, 347–363. <http://dx.doi.org/10.1016/j.enconman.2014.11.014>.
- Costa, S.-C., Mahkamov, K., Kenisarin, M., Lynn, K., Halimic, E., Mullen, D., 2018. Solar Salt Latent Heat Thermal Storage for a small Solar Organic Rankine Cycle Plant. In: *ASME 2018 12th Int. Conf. Energy Sustain. Collocated with ASME 2018 Power Conf. ASME 2018 Nucl. Forum. ASME Pap. No. ES2018-7326, V001T08A002*.
- Costa, K., Kenisarin, M., Ismail, M., Lynn, K., Halimic, E., et al., 2020. Solar Salt Latent Heat Thermal Storage for a small Solar Organic Rankine Cycle Plant. *J. Energy Resour. Technol.* 142.
- Delgado-Torres, A.M., García-Rodríguez, L., 2010. Analysis and optimization of the low-temperature solar organic Rankine cycle (ORC). *Energy Convers. Manage.* 51, 2846–2856. <http://dx.doi.org/10.1016/j.enconman.2010.06.022>.
- Freeman, J., Guarracino, I., Kalogirou, S.A., Markides, C.N., 2017. A small-scale solar organic rankine cycle combined heat and power system with integrated thermal energy storage. *Appl. Therm. Eng.* 127, 1543–1554. <http://dx.doi.org/10.1016/j.applthermaleng.2017.07.163>.
- Gang, P., Jing, L., Jie, J., 2011. Design and analysis of a novel low-temperature solar thermal electric system with two-stage collectors and heat storage units. *Renew. Energy* <http://dx.doi.org/10.1016/j.renene.2011.02.008>.
- Ghaebi, H., Rostamzadeh, H., 2020. Performance comparison of two new co-generation systems for freshwater and power production based on organic Rankine and Kalina cycles driven by salinity-gradient solar pond. *Renew. Energy*.
- Günther, E., Hiebler, S., Mehling, H., Redlich, R., 2009. Enthalpy of Phase Change Materials as a function of temperature : Required accuracy and Suitable Measurement Methods. *Int. J. Thermophys.* 30, 1257–1269. <http://dx.doi.org/10.1007/s10765-009-0641-z>.
- Hasnain, S.M., 1998. Review on sustainable thermal energy storage technologies, Part I: heat storage materials and techniques. *Energy Convers. Manage.* 39, 1127–1138. [http://dx.doi.org/10.1016/S0196-8904\(98\)00025-9](http://dx.doi.org/10.1016/S0196-8904(98)00025-9).
- Iasiello, M., Braimakis, K., Andreozzi, A., Karellas, S., 2017. Thermal analysis of a Phase Change Material for a Solar Organic Rankine Cycle. *J. Phys. Conf. Ser.* 923. <http://dx.doi.org/10.1088/1742-6596/923/1/012042>.
- Iqbal, M.A., Rana, S., Ahmadi, M., Date, A., Akbarzadeh, A., 2020. Experimental study on the prospect of low-temperature heat to power generation using trilateral Flash Cycle (TFC). *Appl. Therm. Eng.* 115139.
- Lacroix, M., 1993. Numerical simulation of a shell-and-tube latent heat thermal energy storage unit. *Sol. Energy* 50, 357–367. [http://dx.doi.org/10.1016/0038-092X\(93\)90029-N](http://dx.doi.org/10.1016/0038-092X(93)90029-N).
- Lakhani, S., Raul, A., Saha, S.K., 2017. Dynamic modelling of ORC-based solar thermal power plant integrated with multitube shell and tube latent heat thermal storage system. *Appl. Therm. Eng.* 123, 458–470. <http://dx.doi.org/10.1016/j.applthermaleng.2017.05.115>.
- Li, J., Alvi, J.Z., Pei, G., Ji, J., Li, P., Fu, H., 2016a. Effect of working fluids on the performance of a novel direct vapor generation solar organic Rankine cycle system. *Appl. Therm. Eng.* 98, 786–797. <http://dx.doi.org/10.1016/j.applthermaleng.2015.12.146>.
- Li, J., Alvi, J.Z., Pei, G., Su, Y., Li, P., Gao, G., et al., 2016b. Modelling of organic Rankine cycle efficiency with respect to the equivalent hot side temperature. *Energy* 115, 668–683. <http://dx.doi.org/10.1016/j.energy.2016.09.049>.
- Li, J., Li, P., Pei, G., Alvi, J.Z., Ji, J., 2016c. Analysis of a novel solar electricity generation system using cascade rankine cycle and steam screw expander. *Appl. Energy* 165, 627–638. <http://dx.doi.org/10.1016/j.apenergy.2015.12.087>.
- Li, J., Li, P., Pei, G., Ji, J., Alvi, J.Z., Xia, L., 2015. A Novel hybrid solar power generation system using a-Si Photovoltaic / Thermal collectors and organic rankine cycle. In: *Proc 3rd Int Semin ORC Power Syst.* pp. 1–10.
- Mago, P.J., Chamra, L.M., Srinivasan, K., Somayaji, C., 2008. An examination of regenerative organic Rankine cycles using dry fluids. *Appl. Therm. Eng.* 28, 998–1007.
- Manfrida, G., Secchi, R., Stańczyk, K., 2016. Modelling and simulation of phase change material latent heat storages applied to a solar-powered Organic Rankine Cycle. *Appl. Energy* 179, 378–388. <http://dx.doi.org/10.1016/j.apenergy.2016.06.135>.
- Marion, M., Voicu, I., Tiffonnet, A.-L., 2014. Wind effect on the performance of a solar organic Rankine cycle. *Renew. Energy* 68, 651–661.
- 23 NSRD, 2010. NIST thermodynamic and transport properties of refrigerants and refrigerant mixtures REFPROP.
- Oyekale, J., Petrollese, M., Cau, G., 2020. Multi-objective thermo-economic optimization of biomass retrofit for an existing solar organic rankine cycle power plant based on NSGA-II. *Energy Rep.* 6, 136–145. <http://dx.doi.org/10.1016/j.egypr.2019.10.032>.
- Pei, G., Li, J., Ji, J., 2010. Analysis of low temperature solar thermal electric generation using regenerative Organic Rankine Cycle. *Appl. Therm. Eng.* 30, 998–1004. <http://dx.doi.org/10.1016/j.applthermaleng.2010.01.011>.
- Quoilin, S., Orosz, M., Hemond, H., Lemort, V., 2011. Performance and design optimization of a low-cost solar organic Rankine cycle for remote power generation. *Sol. Energy* 85, 955–966. <http://dx.doi.org/10.1016/j.solener.2011.02.010>.
- Refiei, A., Loni, R., Najafi, G., Sahin, A.Z., Bellos, E., 2020. Effect of use of MWNT/oil nanofluid on the performance of solar organic Rankine cycle. *Energy Rep.* 6, 782–794. <http://dx.doi.org/10.1016/j.egypr.2020.03.035>.
- Roy, J.P., Mishra, M.K., Misra, A., 2011. Performance analysis of an Organic Rankine Cycle with superheating under different heat source temperature conditions. *Appl. Energy* 88, 2995–3004.
- Sayyaadi, H., Khosravanifard, Y., Sohani, A., 2020. Solutions for thermal energy exploitation from the exhaust of an industrial gas turbine using optimized bottoming cycles. *Energy Convers. Manage.* 207, 112523.
- Sharma, A., Tyagi, V.V., Chen, C.R., Buddhi, D., 2009. Review on thermal energy storage with phase change materials and applications. *Renew. Sustain. Energy Rev.* 13, 318–345. <http://dx.doi.org/10.1016/j.rser.2007.10.005>.
- Tian, Y., Zhao, C.Y., 2013. A review of solar collectors and thermal energy storage in solar thermal applications. *Appl. Energy* 104, 538–553. <http://dx.doi.org/10.1016/j.apenergy.2012.11.051>.
- TVP Solar Datasheet, 2020. HT-Power Product n.d. [https://www.tvpsolar.com/attach/MT-PowerDatasheet\(v4SK\).pdf](https://www.tvpsolar.com/attach/MT-PowerDatasheet(v4SK).pdf) (accessed June 7, 2020).
- Usman, M., Imran, M., Yang, Y., Lee, D.H., Park, B.-S., 2017. Thermo-economic comparison of air-cooled and cooling tower based Organic Rankine Cycle (ORC) with R245fa and R1233zde as candidate working fluids for different geographical climate conditions. *Energy* 123, 353–366. <http://dx.doi.org/10.1016/j.energy.2017.01.134>.
- Voller, V.R., Cross, M., Markatos, N.C., 1987. An enthalpy method for convection/diffusion phase change. *Int. J. Numer. Methods Eng.* 24, 271–284. <http://dx.doi.org/10.1002/nme.1620240119>.
- Wang, X.D., Zhao, L., Wang, J.L., 2011. Experimental investigation on the low-temperature solar Rankine cycle system using R245fa. *Energy Convers. Manage.* 52, 946–952. <http://dx.doi.org/10.1016/j.enconman.2010.08.022>.
- Wang, J.L., Zhao, L., Wang, X.D., 2012. An experimental study on the recuperative low temperature solar Rankine cycle using R245fa. *Appl. Energy* 94, 34–40. <http://dx.doi.org/10.1016/j.apenergy.2012.01.019>.
- Wang, X.D., Zhao, L., Wang, J.L., Zhang, W.Z., Zhao, X.Z., Wu, W., 2010. Performance evaluation of a low-temperature solar Rankine cycle system utilizing R245fa. *Sol. Energy* 84, 353–364. <http://dx.doi.org/10.1016/j.solener.2009.11.004>.
- Xu, G., Song, G., Zhu, X., Gao, W., Li, H., Quan, Y., 2015. Performance evaluation of a direct vapor generation supercritical ORC system driven by linear Fresnel reflector solar concentrator. *Appl. Therm. Eng.* 80, 196–204.